A coupled MMALE-FE method for solving 3D fluid-solid interaction problems with multi-material flow

Xiang Chen and Xiong Zhang
Department of Engineering Mechanics, Tsinghua University, Beijing, China

Received 29 October 2018
Revised 17 December 2018
Accepted 1 January 2019

Abstract

Purpose – The simulation of the fluid–solid interaction (FSI) problem is important for both academic studies and engineering applications. However, the numerical approach for simulating the FSI problems is a great challenge owing to the large discrepancy of material properties and inconsistent description of grid motion between the fluid and solid domains. The difficulties will be further increased if there are multiple materials in the fluid region. In these complicated applications, interface reconstruction, multi-material advection and FSI must be all taken into account. This paper aims to present an effective integrated work of multi-material arbitrary Lagrangian Eulerian (MMALE) method, finite element (FE) method and the continuum analogy method to simulate the complex FSI problems involving multi-material flow. The coupled method is used to simulate the three-dimensional CONT test and the blast-plate interaction. The numerical results show good agreement with the benchmark and the experiment data, which indicates that the presented method is effective for solving the complicated FSI problems.

Design/methodology/approach – MMALE and FE methods are used to simulate fluid and solid regions, respectively. The interfacial nodes of fluid and solid are required to be coincident in the whole simulation so the interacted force can be easily and accurately calculated. To this end, the continuum analogy method is used in the rezoning phase.

Findings – The coupled method is used to simulate the three-dimensional CONT test and the blast-plate interaction. The numerical results show good agreement with the benchmark and the experiment data, which indicates that the presented method is effective for solving the complicated FSI problems.

Originality/value – To the best of the authors' knowledge, this is the first time that the ALE method, moment of fluid interface reconstruction method, continuum analogy method and the FE method are combined to solve complicated practical problems.

Keywords Fluid–solid interaction, Arbitrary Lagrangian Eulerian method, Continuum analogy, Multi-material flow

Paper type Research paper

1. Introduction

The study about the simulation of multi-material flow with fluid–solid interaction problem is very important in practice, such as the structural shielding, weapon design and the safety assessment of the nuclear reactor. However, both fluid solid interaction and multi-material flow are challenge issues in the computational mechanics.

Because the shear and tensile moduli of a fluid material are much lower than a solid material, the fluid material is easy to experience severe deformation during the simulation. Therefore, the Eulerian frame is always used to describe the motion in the fluid region. However, the solid structures are usually described by the Lagrangian frame, so

This work was supported by the National Natural Science Foundation of China (Grant No. 11390363).

Engineering Computations

0264-4401
DOI 10.1108/EC-10-2018-0486

inconsistent description of grid motion makes difficulties in calculating the interaction between the fluid and solid materials. Early numerical approaches for the FSI problem solve the fluid and the solid governing equations alternatingly and the interface conditions are applied asynchronously (Felippa *et al.*, 2001; Piperno and Farhat, 2001; Piperno *et al.*, 1995). These partitioned methods are usually energy increasing and unstable near the fluid solid interface (Piperno *et al.*, 1995). To obtain the higher accuracy, the monolithic methods, which update the fluid and solid region simultaneously, are developed, and the Arbitrary Lagrangian Eulerian method (ALE) is most famous approach (Donea *et al.*, 1982; Hu *et al.*, 2001; Liu and Ma, 1982; Zhang *et al.*, 2003). In the ALE frame, the motion of grid is defined as an independent degree of freedom, so the best properties of Lagrangian and Eulerian frames are preserved. In the past years, the ALE method has been widely used for its accuracy, robustness and efficiency (Benson, 1992; Hirt *et al.*, 1997; Kjellgren and Hyvarinen, 1998; Luo *et al.*, 2004; Vitali and Benson, 2006).

Usually, the ALE frame used in the fluid–solid interaction simulation is realized by solving the governing equation on a moving coordinate system (Hu *et al.*, 2001; Huerta and Liu, 1988; Liu and Ma, 1982). The velocity of the nodes on the fluid–solid interface equals to the local material velocity, so the fluid–solid interface can be innately tracked in the Lagrangian frame. The velocity of the other nodes in the fluid region is calculated from the rezone algorithm (Knupp *et al.*, 2002 and Huerta and Liu, 1988) to preserve the high quality of the grid. The rezone and advection should be performed at every step which is time consuming especially for 3 D simulation. Moreover, the traditional advection methods are also difficult to simulate the multi-material flow because they cannot accurately calculate the flux of each material (Kucharik and Shashkov, 2014).

The other way to implement the ALE method is the splitting operators approach. It separates the ALE method into three steps, namely, the Lagrangian phase, the rezoning phase and the remapping phase. In the Lagrangian phase, the governing equations in Lagrangian frame are solved and neither rezone nor advection is required in this phase. It is easy to couple the fluid and solid interaction in the Lagrangian phase because the same grid motion description is used. The fluid grid can be severely distorted after several Lagrangian steps, and a rezoning phase should be performed to generate a new grid with high quality. Then, the physical variables are interpolated from the old grid to the new grid in the remapping phase. And finally, the Lagrangian phase continues on the new grid until the grid distortion appears again. The splitting operators approach is widely used for the fluid simulation in recent years because of the great developments about the Lagrangian fluid dynamics (Caramana *et al.*, 1998; Caramana *et al.*, 1998; Kolev and Rieben, 2009; Loubere *et al.*, 2013; Caramana and Loubere, 2006) and the remapping algorithms (Garimella *et al.*, 2007; Grandy, 1999; Kucharik *et al.*, 2003). However, to our knowledge, less attention is paid on the usage of splitting operators approach for fluid–solid interaction simulation.

The other topic of this work is about the multi-material flow, which refers to the attendance of at least two different materials in the fluid region, so the fluid-fluid interface must be tracked. Although the fluid-fluid interface could be tracked in the same way as the fluid–solid interface, the severe deformation of fluid-fluid interface will induces large difficulties in the rezoning phase. In some extreme cases where the topology of the fluid-fluid interface changes, it is almost impossible to smooth the grid successfully. To solve the problem, the Multi-Material ALE method (MMALE) is developed which introduces mix cells to allow multiple materials attending in a single cell (Galera *et al.*, 2011; Galera *et al.*, 2010; Jia *et al.*, 2013; Luo *et al.*, 2004; Peery and Carroll, 2000). Therefore, the fluid-fluid interface is able to pass through the mix cell and the difficulties in the rezoning phase can be avoided in

essence because the location of the fluid-fluid interface does not affect the rezoning phase any more. However, the attendance of mix cells leads to other challenges such as the closure model (Barlow *et al.*, 2014; Shashkov, 2008; Yanilkin *et al.*, 2013), the interface reconstruction (Benson, 2002; Fedkiw *et al.*, 1999; Fedkiw *et al.*, 1999; William and Douglas, 1998) and the multi-material remapping (Berndt *et al.*, 2010; Kucharik and Shashkov, 2012; Kucharik and Shashkov, 2014). In recent years, there are numerous research presented to solve these problems and the MMALE method has been successfully implemented in simulating three dimensional complicated multi-material flow (Chen *et al.*, 2017; Jia *et al.*, 2013).

The MMALE method is usually realized via splitting operators approach which is also feasible for fluid–solid interaction, so it shows great potential for solving more complicated problems. This paper attempts to present an integrated work of the MMALE method, Finite Element (FE) method and the continuum analogy method to simulate the complex FSI problems involving multi-material flow. In the coupled MMALE-FE method, the fluid and solid region are simulated by MMALE and FE method, respectively and the continuum analogy method (Yoseph *et al.*, 2001) is used in the rezoning phase. The coupled MMALE-FE method is then applied to simulate the three dimensional CONT test (Benuzzi, 1987) and the blast-plate interaction (Neubergera *et al.*, 2007). The numerical results show good agreement with the benchmark and the experiment data, which indicates that the presented method is effective for solving the complicated FSI problems.

It should be mentioned that other advanced numerical approaches may also be able to simulate the FSI problem with multi-material flow. For instance, the CFEMP (Coupled Finite Element Material Point) method (Chen *et al.*, 2015; Lian *et al.*, 2011; Lian *et al.*, 2014; Lian *et al.*, 2012), which uses material points to represent the fluid material and the FM method to simulate the solid structure. The fluid–solid interaction is calculated from the contact between the fluid particles and the solid elements. However, the CFEMP method may suffer from the problems about the lower accuracy in the fluid simulation and the particle leak in the contact algorithm (Zhang *et al.*, 2017). Immersed Finite Element Method (IFEM) (Liu *et al.*, 2006; Zhang *et al.*, 2004) is another choice for simulating complicated FSI problems. The solid grid is immersed into the fluid grid and they are overlapped, so the rezoning phase in the ALE frame can be avoided. The interaction between fluid and solid region is obtained from the high order interpolation of the velocity and stress field between the solid and fluid grid. IFEM is suitable for simulating the FSI problems with large rigid movement of the solid material, but the numerical results may be unreliable in the case involving large solid deformation (Wang and Zhang, 2013).

The remaining part of the paper is organized as follows. In Section 2 and 3, the basic idea of the MMALE and FE method are briefly reviewed. Section 4 introduces the algorithm for the fluid–solid coupling including the consistent of interacted force, the time integration and the rezoning. Two numerical examples are presented in Section 5, which contains a benchmark test in nuclear reactor safety evaluation and an air blast-circular plate interaction with experiment data. Finally, the conclusions are summarized in Section 6.

2. The MMALE method for fluid region

In this section, we will briefly review the major process of multi-material ALE method, namely, the Lagrangian phase, the surface reconstruction phase and the multi-material remapping phase. The rezoning phase will be introduced in the next section because it is related to the fluid–solid interaction scheme.

2.1 Lagrangian phase

The fluid region is described in Lagrangian frame and the governing equations are:

$$\frac{\mathrm{d}\rho}{\mathrm{d}t} = -\rho\nabla\cdot\boldsymbol{v} \tag{1}$$

$$\rho\frac{\mathrm{d}\boldsymbol{v}}{\mathrm{d}t} = -\nabla P \tag{2}$$

$$\rho\frac{\mathrm{d}e}{\mathrm{d}t} = -P\nabla\cdot\boldsymbol{v} \tag{3}$$

The staggered grid, where the position and velocity are stored at the nodes while the density, specific internal energy and pressure are stored at the cell center, is used to discretize the fluid region. In the past two decades, many efforts have been taken for the sake of an accurate, stable and robust formulation to simulate the behavior of fluid materials in Lagrangian frame and the compatible discretization (Caramana *et al.*, 1998; Caramana *et al.*, 2000) should be the most important one. A brief introduction of the compatible discretization is presented in the following.

Figure 1 shows four cells, namely, z_1, z_2, z_3 and z_4, in the fluid region. Each cell is divided into four corner volumes denoted as Ω_m^n, where m is cell where the corner volume locates and n is the node that the corner volume connects to. The controlling volume of a node is defined as the sum of the connected corner volumes. For instance, the controlling volume of node p_1 in Figure 1 is:

$$\Omega^{p_1} = \sum_i \Omega_{z_i}^{p_1} \tag{4}$$

Integrating equation (2) on Ω^{p_1} and applying the Gauss's theory, the discretization of the momentum equation is:

$$M^{p_1}\frac{\mathrm{d}\boldsymbol{v}^{p_1}}{\mathrm{d}t} = -\oint_{\partial\Omega^{p_1}} P\mathrm{d}\boldsymbol{l} = -\sum_i P_{z_i}\int_{S_{z_i}^{p_1}}\mathrm{d}\boldsymbol{l} = \sum_i \boldsymbol{f}_{z_i}^{p_1} \tag{5}$$

where M^{p_1} is the nodal mass which equals to the mass of the controlling volume, and $S_{z_i}^b$ is the subset of $\partial\Omega^b$ that inside the cell z_i. $\boldsymbol{f}_{z_i}^{p_1}$ is named as the corner force of z_i.

Substituting equation (5) into equation (3) and applying the energy conversation law of the system, the discretization of the energy equation is:

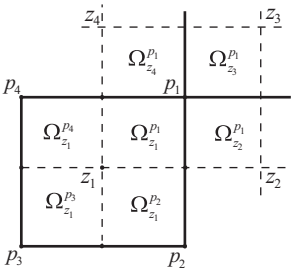

Figure 1.
The illustration of staggered grid and compatible discretization in Lagrangian phase

$$M_{z_1}\frac{\mathrm{d}e_{z_1}}{\mathrm{d}t}=-\sum_j \boldsymbol{f}_{z_1}^{p_j} \tag{6}$$

where M_{z_1} is the cell mass which equals to the sum of the corner masses inside cell z_1.

It should be emphasized that the discretization of the momentum and energy equations are compatible because the energy conservation of the system can be rigorously preserved, so equation (5) and equation (6) are named as the "compatible discretization."

The predictor-corrector scheme (52) is used for the time integration, namely:

$$M^{p_1}\frac{\boldsymbol{v}^{p_1,n+1}-\boldsymbol{v}^{p_1,n}}{\Delta t}=\sum_i \boldsymbol{f}_{z_i}^{p_1,n+1/2} \tag{7}$$

$$M_{z_1}\frac{e_{z_1}^{n+1}-e_{z_1}^{n}}{\Delta t}=-\sum_j \boldsymbol{f}_{z_1}^{p_j,n+1/2}\cdot\boldsymbol{v}_c^{p_j,n+1/2} \tag{8}$$

In practice, the grid is firstly updated to the $n+1/2$ step to estimate pressure and corner force at the middle step, and then all physical quantities are updated to the full time step. It should be mentioned here that the predictor-corrector scheme should also be used in the solid region to guarantee the coincidence of the nodes at the fluid–solid interface during the Lagrangian step and it will be specifically discussed in Section 4.2.

The artificial viscosity is applied to provide the entropy production and introduce dissipation for shock discontinuity (Caramana *et al.*, 1998; Kolev and Rieben, 2009), and the hourglass viscosity is also used to eliminate hourglass motion and spurious vorticity (Caramana and Shashkov, 1998). For the mixed cells in the MMALE, the Tipton pressure relaxation model (Shashkov, 2008) is used to determine the pressure in mixed cells. Finally, the material centroid should also be updated in Lagrangian phase for the fluid-fluid interface reconstruction and we use the constant parametric coordinate method (Kucharik *et al.*, 2010).

2.2 Interface reconstruction phase

The fluid-fluid interface should be reconstructed to distinguish different fluid materials. The frequency of performing the interface reconstruction phase depends on the closure model. If the closure model requires the information of the interface location (Barlow *et al.*, 2014), the interface must be reconstructed at every time step. However, the Tipton pressure relaxation model used in this paper does not need the interface location information, so the interface reconstruction phase only performs before the remapping phase when the grid is severely distorted.

PLIC (Piecewise Linear Interface Calculation) method is usually used in the MMALE method for the interface reconstruction which constructs a plane in the mix cell to represent the fluid-fluid interface. In this paper, the moment of fluid (MoF) method (Ahn and Shashkov, 2007; Chen and Zhang, 2016; Chen and Zhang, 2017) is used and it is an advanced interface reconstruction algorithm with higher accuracy compared with the traditional PLIC-VoF method (Kucharik *et al.*, 2010). Moreover, it does not need any information from the neighbor cells which allows it to be implemented as a cell-by-cell black-box routine and be parallelized innately.

The optimal linear interface calculated by the MoF method should fulfill two requirements: 1. the truncation volume from the interface must precisely equal to the given

reference material volume and 2. The discrepancy between the given reference material centroid and the truncation centroid should be minimized by the optimal interface. Therefore, the mathematic expression of the MoF method can be described as: calculating a particular plane $n^* x + d^* = 0$ to minimize the objective function:

$$f(\boldsymbol{n}, d) = \|\boldsymbol{x}(\boldsymbol{n}, d) - \boldsymbol{x}^{\text{ref}}\|^2 \tag{9}$$

subject to the volume condition:

$$v(\boldsymbol{n}, d) = v^{\text{ref}} \tag{10}$$

where $x(\boldsymbol{n}, d)$ and $v(\boldsymbol{n}, d)$ are the centroid and volume below the truncation polyhedron by the approximate interface, and x^{ref} and v^{ref} are the given reference material centroid and volume in the mixed cell, respectively.

2.3 Multi-material remapping phase

After the interface reconstruction process, the old grid is decomposed into non-overlapping polyhedrons and each polyhedron only contains one material. We call them as the material polyhedrons (MPs). Before remapping, the density ρ, specific internal energy e and pressure p are stored at the centroid of the MPs while the velocity is stored at nodes of the old grid. The purpose of the remapping phase is to determine the physical variables, including the material density, internal energy, velocity, volume fraction and material centroid, in the new grid generated from the rezoning phase.

The intersection based remapping (Chen *et al.*, 2017; Grandy, 1999; Jia *et al.*, 2013) must be used to interpolate the volume fraction and the material centroid to avoid unphysical phenomena such as negative mass and pseudo fragmentation (Kucharik and Shashkov, 2014). In the intersection based method, every cell in the new grid intersects with the MPs in the old grid, and then accumulates the mass, internal energy, volume and moment of the intersecting portion. Taking the interpolation of the volume fraction and the material centroid as an example, the volume and moment of kth material in jth cell of the new grid equals to:

$$V_k(C_j) = \sum_i V\left(C_j \cap P_k^i\right) i \in \left\{i | C_j \cap P_k^i \neq \varnothing\right\} \tag{11}$$

$$M_k(C_j) = \sum_i M\left(C_j \cap P_k^i\right) i \in \left\{i | C_j \cap P_k^i \neq \varnothing\right\} \tag{12}$$

where C_j is the jth cell of the new grid, and P_k^i is the MP for the kth material in the ith cell of the old grid.

Subsequently, the volume faction and centroid of the kth material in C_j is:

$$v_k(C_j) = \frac{V_k(C_j)}{V(C_j)} \tag{13}$$

$$\boldsymbol{x}_k(C_j) = \frac{M_k(C_j)}{V_k(C_j)} \tag{14}$$

where $V(C_j)$ is the volume of C_j. Other physical variables such as density, specific internal energy and velocity can be interpolated in the similar way.

The above algorithm is used to remapping the cell-centered variables, such as the density, specific internal energy and the volume fraction. To remap the velocity, the controlling volume of the nodes in the new and old grid, namely, Ω^j_{old} and Ω^i_{new}, are intersected and the momentum carried by the intersection portion is:

$$\boldsymbol{p}\left(\Omega^i_{\text{new}} \cap \Omega^j_{\text{old}}\right) = \boldsymbol{v}^j_{\text{old}} m\left(\Omega^i_{\text{new}} \cap \Omega^j_{\text{old}}\right) \tag{15}$$

where $m\left(\Omega^i_{\text{new}} \cap \Omega^j_{\text{old}}\right)$ is the mass of the intersection portion which can be calculated when remapping the density, and $\boldsymbol{v}^j_{\text{old}}$ is the velocity of the node j in the old grid. The mass and momentum of Ω^i_{new} can be calculated from the sum of the intersection portions, namely:

$$m\left(\Omega^i_{\text{new}}\right) = \sum_j m\left(\Omega^i_{\text{new}} \cap \Omega^j_{\text{old}}\right)$$
$$\boldsymbol{p}\left(\Omega^i_{\text{new}}\right) = \sum_j \boldsymbol{p}\left(\Omega^i_{\text{new}} \cap \Omega^j_{\text{old}}\right)$$

and finally, the node velocity in the new grid is:

$$\boldsymbol{v}^j_{\text{new}} = \frac{\boldsymbol{p}\left(\Omega^i_{\text{new}}\right)}{m\left(\Omega^i_{\text{new}}\right)} \tag{16}$$

The advantages of the intersection based remapping is obvious. Firstly, the volume fraction and material centroid in the new cells are directly calculated from the configurations of different materials form the old grid, rather than calculating the material flux. So it avoids the drawbacks of the flux based remapping such as negative mass and unphysical material fragments in essence. Secondly, different from the flux based remapping where the new and old grid must be close to each other to calculate the appropriate flux region, the topology of the old and new grid can even be different in the intersection based remapping. This property significantly increase the flexibility in the rezoning phase.

The key technique of the intersection based remapping is an accurate, efficient and robust calculation of the intersection portion of any two arbitrary polyhedrons. This issue has been well settled by the "Clipping and Capping" method (Chen *et al.*, 2017).

3. Finite element method for solid region

In this paper, the solid region is described in Lagrangian frame and governed by the conservative low as:

$$\dot{\rho} = -\rho \nabla \cdot \boldsymbol{v} \tag{17}$$

$$\rho \ddot{\boldsymbol{x}} = \nabla \cdot \boldsymbol{\sigma} + \rho \boldsymbol{f}^{\text{ext}} \tag{18}$$

$$\rho \dot{e} = \dot{\boldsymbol{\varepsilon}} : \boldsymbol{\sigma} \tag{19}$$

The finite element (FE) method is used to solve equation (17) to equation (19) and the 8-node hexahedral element and the Belytschko–Lin–Tsay (BLT) shell element (Belytschko *et al.*, 1983; Belytschko *et al.*, 1991) are employed to discretize the solid region.

For the 8-node hexahedral element, the degree of freedom (DoF) at each node is $x = (x, y, z)$ and the shape functions of the element are:

$$N_i = \frac{1}{8}\left(1 + (-1)^i \xi\right)\left(1 + (-1)^{\left[\frac{i+1}{2}\right]} \eta\right)\left(1 + (-1)^{\left[\frac{i+3}{2}\right]} \zeta\right) \tag{20}$$

Deriving from the weak form of equation (18), the momentum equation can be rewritten as:

$$M_i \ddot{\boldsymbol{x}}_i = \boldsymbol{f}_i^{\text{int}} + \boldsymbol{f}_i^{\text{ext}} \tag{21}$$

where m_i is the mass of node i, and $\boldsymbol{f}_i^{\text{int}}$ $\boldsymbol{f}_i^{\text{ext}}$ are the internal and external force applied on node i, respectively.

For the BLT shell element, the DoF at each node is $(\boldsymbol{x}, \boldsymbol{\theta}) = (x, y, z, \theta_x, \theta_y, \theta_z)$ and the shape functions of the element are:

$$N_i = \frac{1}{8}\left(1 + (-1)^i \xi\right)\left(1 + (-1)^{\left[\frac{i+1}{2}\right]} \eta\right) \tag{22}$$

The velocity along the thickness is assumed as:

$$\boldsymbol{v}(\hat{z}) = \boldsymbol{v}^{\text{m}} - \hat{z}\boldsymbol{e}_3 \times \dot{\boldsymbol{\theta}} \tag{23}$$

where $\boldsymbol{v}_i^{\text{m}} = \dot{\boldsymbol{x}}$ is the velocity at the neutral plane, and $\boldsymbol{e}_3$ is the normal of the shell element, and $\hat{z}$ is the coordinate alone the shell thickness. Deriving from the weak form of equation (18), the momentum equation can be rewritten as:

$$M_i^{\text{T}} \ddot{\boldsymbol{x}}_i = -\boldsymbol{f}_i^{\text{int}} + \boldsymbol{f}_i^{\text{ext}} \tag{24}$$

$$\underset{M}{{}^{i\text{R}}} \ddot{\boldsymbol{\theta}}_i = -\boldsymbol{m}_i^{\text{int}} + \boldsymbol{m}_i^{\text{ext}} \tag{25}$$

where M_i^{T}, M_i^{R} are the mass and rotational inertia of node i, and $\boldsymbol{f}_i^{\text{int}}$, $\boldsymbol{m}_i^{\text{int}}$ are the internal force and moment applied on node i, and f_i^{ext}, $\boldsymbol{m}_i^{\text{ext}}$ are the external force and moment applied on node i.

The time integration of the FE method should be consistent with the MMALE method, and it will be specifically introduced in Section 4.2.

4. Fluid–solid interaction model and the continuum analogy method

In this section, we will introduce the coupling strategy of the MMALE method in the fluid domain and the FE method in the solid domain by the co-node approach. Co-node means the nodes at the interface of the fluid and solid regions are always coincident during the whole simulation and it implies the non-slipping boundary condition at the fluid–solid interface. The superiority of the co-node approach is the interacted force of the fluid and solid material can be accurately calculated, as shown in Section 4.1. Moreover, the time integration scheme

of the fluid and solid region must be the same to insure the co-node requirement in Lagrangian step, and this issue is discussed in Section 4.2. Finally, the coincidence of the interfacial nodes should be preserved after the remapping phase, which implies that the grid in the fluid region can just be smoothed with the interfacial nodes fixed. To this end, the continuum analogy method is used in Section 4.3.

4.1 Interacted force consistency

Figure 2(a) shows the interface of the fluid and solid region. C_1 and C_2 are occupied by the fluid material while C_3 and C_4 are occupied by the solid material. S_1 and S_2 are the fluid–solid interface of these four cells and they share a common node A. To calculate the interacted force at node A, the fluid and solid region are analyzed individually as shown in Figure 2(b). In the fluid region, the nodal mass and force of A^{Fluid}, namely, m^{Fluid} and $\boldsymbol{f}^{\text{Fluid}}$, are contributed from C_1 and C_2, and they can be directly calculated from the configuration, density and stress of the two cells. Similarly in the solid region, the nodal mass and force from C_3 and C_4 are m^{Solid} and $\boldsymbol{f}^{\text{Solid}}$, respectively. Besides $\boldsymbol{f}^{\text{Fluid}}$ and $\boldsymbol{f}^{\text{Solid}}$, the interacted force between the fluid and solid region is also applied on A^{Fluid} and A^{Solid}, namely, the $\boldsymbol{f}^{\text{interacted}}$ alone the dashed line with opposite directions in Figure 2.

Therefore, the accelerations of A^{Fluid} and A^{Solid} are:

$$\boldsymbol{a}^{\text{Fluid}} = \frac{\boldsymbol{f}^{\text{Fluid}} + \boldsymbol{f}^{\text{interacted}}}{m^{\text{Fluid}}} \tag{26}$$

$$\boldsymbol{a}^{\text{Solid}} = \frac{\boldsymbol{f}^{\text{Solid}} - \boldsymbol{f}^{\text{interacted}}}{m^{\text{Solid}}} \tag{27}$$

Because the non-slipping boundary condition is applied on the fluid–solid interface, $\boldsymbol{a}^{\text{Fluid}}$ should be equal to $\boldsymbol{a}^{\text{Solid}}$ and $f^{\text{interacted}}$ is solved as:

$$\boldsymbol{f}^{\text{interacted}} = \frac{\boldsymbol{f}^{\text{Solid}} m^{\text{Fluid}} - \boldsymbol{f}^{\text{Fluid}} m^{\text{Solid}}}{m^{\text{Solid}} + m^{\text{Fluid}}} \tag{28}$$

Finally, substitute equation (28) into equation (26) or equation (27) to calculate the acceleration of the A as:

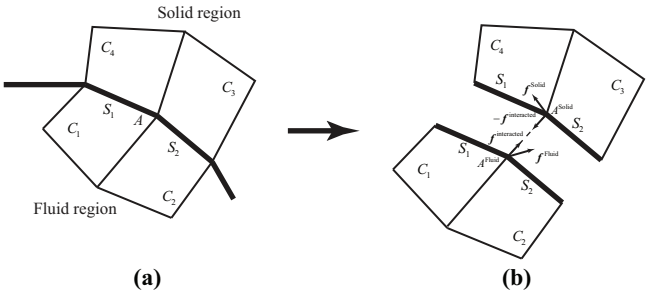

Figure 2.
The interacted force between the fluid and the solid region

$$\boldsymbol{a}^{A} = \boldsymbol{a}^{\text{Fluid}} = \boldsymbol{a}^{\text{Solid}} = \frac{\boldsymbol{f}^{\text{Solid}} + \boldsymbol{f}^{\text{Fluid}}}{m^{\text{Solid}} + m^{\text{Fluid}}} \tag{29}$$

4.2 Time integration consistency

The interacted force in equation (28) results in the same acceleration on the fluid–solid interfacial nodes. However, to guarantee the coincidence after a time step, a same time integration scheme must be used for both fluid and solid region. As described in Section 2.1, the compatible discretization is the most important formula for a conservative simulation and it is incorporated with the predictor-corrector time integration scheme. Therefore, the solid region should also use the predictor-corrector scheme to perform time integration. Figure 3 shows the details of the predictor-corrector scheme in the coupled MMALE-FE method and it can preserve the coincidence of the fluid–solid interfacial nodes during the Lagrangian phase.

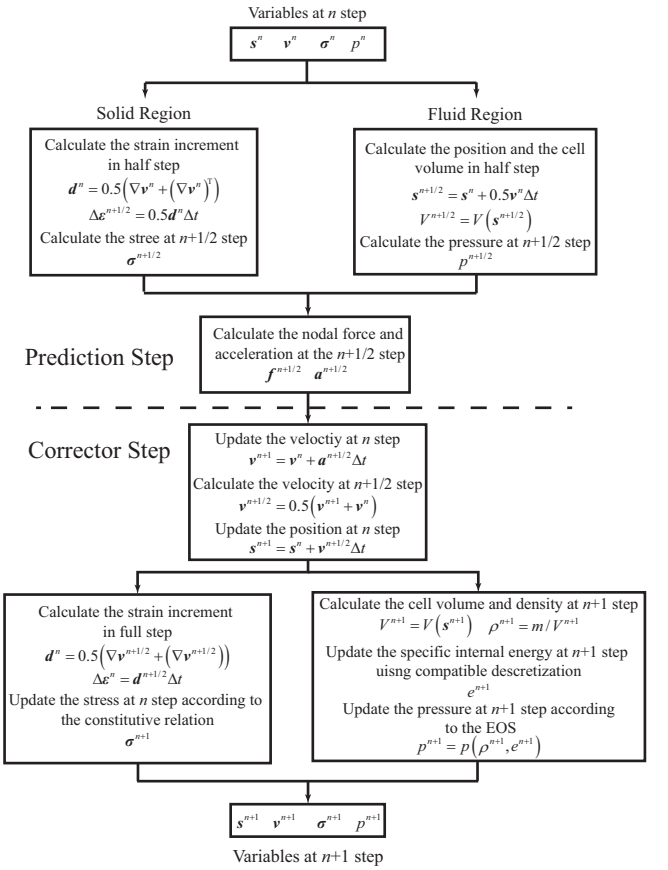

Figure 3.
The time integration scheme in the coupled MMALE-FE method

4.3 Rezone consistence and the continuum analogy method

4.3.1 The rezone consistence requirement. The interacted force in equation (28) incorporating with the uniform time integration scheme in Figure 3 preserves the coincidence of the fluid–solid interfacial nodes in the Lagrangian phase. But for the whole simulation, special consideration must be taken in the rezoning phase. A new grid with higher quality is generated if the old grid is distorted severely. In the FSI simulation, the deformation of the solid region is relatively moderate, so the remapping phase is only performed on the fluid region. Therefore, the nodes in the solid region, including the fluid–solid interfacial nodes, will not be moved in the rezoning phase. It implies that the interfacial nodes must be fixed and only the internal nodes in the fluid region are allowed to move when generating a new grid in the rezoning phase. This is the rezone consistence requirement and Figure 4 shows an example about the interaction between a soft shell and a shock wave. The red line in Figure 4 represents the shell and other cells represent the fluid region. The shell is deformed owing to the interaction and the grid in the fluid region is severely distorted as shown in Figure 4(a). It can be seen that the nodes on the shell are also the nodes of the fluid region, so they are coincident before the rezoning phase. Figure 4(b) shows one of the new generated grids that fulfills the rezone consistence requirement. The nodes on the red line are not moved, so the fluid–solid interfacial nodes are also coincident in the new grid. Finally, after the remapping phase described in Section 2.3, the Lagrangian phase is performed on the new grid and the coincidence of the interfacial nodes can be preserved in the whole simulation.

4.3.2 The continuum analogy method. Because the geometric configuration of the fluid–solid interface is arbitrary, the pseudo structure method seems to be the best way to perform the consistent rezone (Blom, 2000; Yoseph *et al.*, 2001). This method regards the grid as a pseudo structure with pseudo material properties and then solves the equilibrium equation to calculate the coordinates of the new grid. The pseudo material properties of each cell can be different for a better rezone quality. The consistent rezone can be easily achieved by specifying the nodes' displacement on the fluid–solid interface. Spring analogy (Blom, 2000) and the continuum analogy (Yoseph *et al.*, 2001) are two approaches in the pseudo structure method, which regard the grid as a spring system and continuum system, respectively. The continuum analogy is used in this work due its better performance in deformation and grid quality.

The equilibrium equation of the continuum system can be established by the FE method as:

$$\boldsymbol{K}\boldsymbol{d} = \begin{bmatrix} \boldsymbol{K}^{\mathrm{II}} & \boldsymbol{K}^{\mathrm{IB}} \\ \boldsymbol{K}^{\mathrm{BI}} & \boldsymbol{K}^{\mathrm{BB}} \end{bmatrix} \begin{bmatrix} \boldsymbol{d}^{\mathrm{I}} \\ \boldsymbol{d}^{\mathrm{B}} \end{bmatrix} = \begin{bmatrix} \boldsymbol{0} \\ \boldsymbol{0} \end{bmatrix} \tag{30}$$

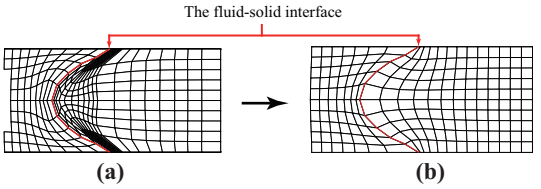

Notes: The red line is the solid region, and it is not moved during the rezoning phase

Figure 4.
The consistent rezone example

where $\boldsymbol{K}$ is the stiffness matrix of this pseudo structure, $\boldsymbol{d}^{\mathrm{I}}$ is the displacement of interior nodes to be solved and $\boldsymbol{d}^{\mathrm{B}}$ is the given displacement at the fluid–solid interface. Equation (30) can be rewritten as linear equations:

$$\boldsymbol{K}^{\mathrm{II}}\boldsymbol{d}^{\mathrm{I}} = -\boldsymbol{K}^{\mathrm{IB}}\boldsymbol{d}^{\mathrm{B}} \tag{31}$$

and the solution $\boldsymbol{d}^{\mathrm{I}}$ is used to determine the nodes of the new grid.

It should be mentioned that if the displacement of the interfacial nodes is large, the solution of equation (31) may lead to illegal cells. For the same example in Figure 4, Figure 5(a) is the new grid generated by solving equation (31) with a uniform pseudo material property. Because the displacement of the fluid–solid interface is large in this example, some illegal cells appear near the interface. To overcome this problem, we use a consolidation process in the rezoning phase. The target displacement of the fluid–solid interface $\boldsymbol{d}^{\mathrm{I}}$ is applied gradually in N steps to the equilibrium equation. In each step, only $\boldsymbol{d}^{\mathrm{I}}/N$ is applied on the RHS of equation (31) to obtain a temporary grid $\boldsymbol{G}^{\mathrm{temp}}$. $\boldsymbol{G}^{\mathrm{temp}}$ is used to calculate $\boldsymbol{K}^{\mathrm{II}}$ and $\boldsymbol{K}^{\mathrm{IB}}$ in the next step, so it just like the temporary grid is consolidated after each step. The consolidation process strengths the stiffness of the cell so the illegal cells can be avoided. Figure 5(b) is the result with $N = 3$ and no illegal cell occurs with the consolidation process. In practice, two or three times of consolidation process is adequate to eliminate the illegal cells.

5. Numerical examples

5.1 CONT benchmark

The LMFBR (liquid metal fast-breeder reactor) is an advanced nuclear reactor that is able to produce more fissile product than it takes in. Therefore, it exhibits remarkable fuel economy compared to traditional light water reactors. When evaluating the safety of a LMFBR, the core disruptive accidents (CDA) is the greatest threat to the reactor. In a CDA, the core of the nuclear reactor melts partially because of some unexpected accidents. And then the chemical interaction between molten fuel and liquid sodium will create a high-pressure gas bubble. The expansion of this bubble impacts the reactor vessel and the internal components, thus leading to great threat to the safety of the reactor (Robbea *et al.*, 2003). Although the probability of the occurrence of CDA is extremely low, the consequences of such accidents, especially the analysis about the primary containment, is required to evaluate the residual risks to the public (Benuzzi, 1987).

It is impossible to study CDA experimentally, so the analysis mainly rely on the numerical simulation. However, CDA is an extremely complicated phenomenon which involves strong impact, multi-material flow and fluid–solid interaction. So to increase confidence of the code capabilities, a benchmark calculation exercise named as CONT was

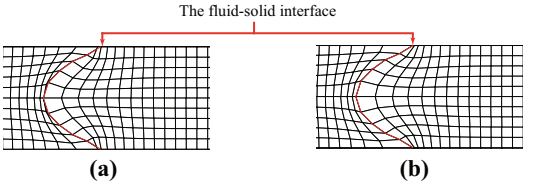

Figure 5.
(a) The illegal cells appeared because of the large fluid–solid interface deformation and (b) the elimination of the illegal cells by using consolidation process

sponsored by the containment loading and response group. In this project, a two dimensional full-size LMFBR undergoing a postulated CDA is defined and the model is submitted to seven codes to perform the simulation. The results of these codes is published by Benuzzi (Benuzzi, 1987), so this problem can be used to verify the validity of our coupled MMALE-FE method.

Figure 6 is the postulated CDA defined in CONT. The realistic problem is simplified as a two dimensional model because the seven codes in the project are only able to perform the 2 D simulation. Moreover, none of the seven code can do the full coupled simulation between different materials and they use some approximate model to simplify the fluid–solid interaction and the multi-material flow. For the details of the codes, the reader can refer to the origin paper (Benuzzi, 1987).

To demonstrate the advantages of the proposed coupled MMALE-FE method, a 3 D model of the CONT test is created as shown in Figure 7 with the same material properties. The fluid region is discretized into 5.4×10^5 hexahedral elements and the inner and outer vessels are discretized into 1.0×10^4 shell elements. Different variables, such as the outer vessel deformation, cover gas pressure and impact velocity, are calculated and compared with the results from the seven codes in the project.

Figure 8 shows the deformation of the outer vessel at the terminate time (a) and the time curve of the pressure at the center of the cover gas (b). The black lines are the results from the project and they are similar to each other. The result from the MMALE-FE method is marked in red line and it matches well with the other results.

Some other variables are quantitatively compared in Table I, and the results from this work are also in the reasonable range according to the reference.

5.2 Blast-plate interaction

This numerical example is about the interaction between an air blast and a circular plate. This problem has been studied experimentally by Neuberger (Neubergera *et al.*, 2007) with the devices shown in Figure 9(a). They conducted series of experiments with different plate

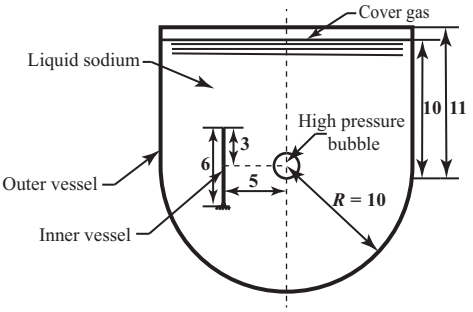

(a)

The EOS of liquid sodium

$p = a_1\mu + a_2\mu/\mu/ + E(b_0 + b_1\mu)$

with: $\mu = \rho/\rho_0 - 1$

$\rho_0 = 832\ \text{kg/m}^3$ $a_1 = 4.44\times10^3$ Pa $a_2 = 4.328\times10^9$ Pa

$b_0 = b_1 = 1.218$

The EOS of high pressure bubble

$$p = p_0\left(\frac{\rho}{\rho_0}\right)^{\gamma}$$

with: $p_0 = 10^7$ Pa ρ_0=2427.8 kg/m^3 $\gamma = 0.75$

The EOS of the cover gas

$$p = p_0\left[\left(\frac{\rho}{\rho_0}\right)^{\gamma} - 1\right]$$

with: $p_0 = 10^5$ Pa ρ_0=10.78 kg/m^3 $\gamma = 1.67$

The material property of the vessel

$E = 1.6\times10^{11}$ Pa $E_p = 1.6\times10^{10}$ Pa

$\rho = 7800\ \text{kg/m}^3$ $\nu = 0.333$ $\sigma_y = 1.05\times10^8$ Pa

(b)

Figure 6.
The geometric model (a) and the material properties (b) in the CONT benchmark

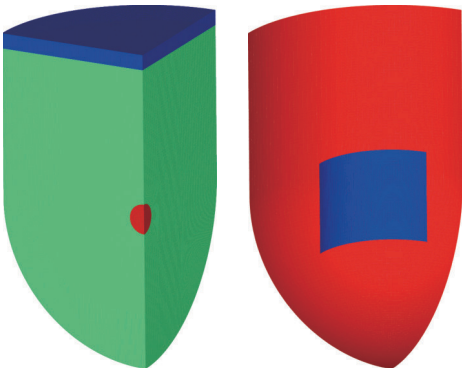

Figure 7.
The 3D model of the CONT benchmark

Notes: (a) is the fluid region including three different materials; (b) is the solid region including the outer and inner vessel

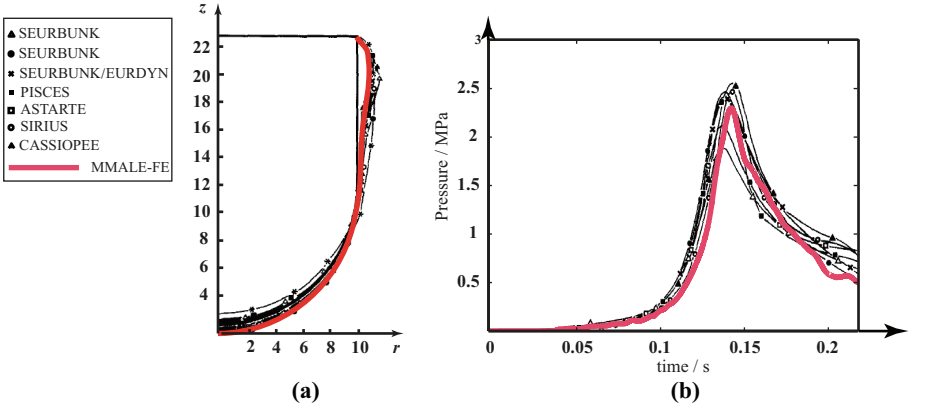

Figure 8.
The comparison of the outer vessel deformation (a) and the time curve of the cover gas pressure (b)

Table I.
The quantitative comparison of the results with the reference

Variables	CONT project	MMALE-FE
Energy release	0.345-0.377 GJ	0.358 GJ
Impact velocity	11.3-14.8 m/s	14.0 m/s
Peak pressure of the cover gas	1.9-2.6 Mpa	2.3 MPa
Strain energy of vessels	0.173-0.219 GJ	0.176 GJ

and explosive sizes and recorded the maximal vertical displacement of the plate of each experiment. In this section, we simulate one of their experiments and simplify it as shown in Figure 9(b) according to the symmetry of this problem. In this example, the diameter of the circular plate is $D = 0.5$ m with thickness $t = 0.01$ m. The distance between the explosive

center and the plate is $R = 0.1$ m and the radius of the explosive is $r = 0.041$ m, namely, 0.486 kg.

The fluid and solid grid is shown in Figure 10 and both of them are discretized into hexahedral elements. Because the explosive is very close to the plate, a refined mesh should be used near the explosive to avoid the severely numerical dissipation. On the other hand, we use a coarse mesh in the far-field to save the calculation time. The number of fluid elements is 3.3×10^5 and the number of solid elements is 2.16×10^4. The terminal time is $t = 0.5$ ms and the maximal vertical displacement of the plate has been reached before this time.

The JWL equation of state is used to describe the explosive products (Liu *et al.*, 2003) as shown in equation (32):

$$p = A\left(1 - \frac{\omega}{R_1 V}\right)e^{-R_1 V} + B\left(1 - \frac{\omega}{R_2 V}\right)e^{-R_2 V} + \omega \rho e \tag{32}$$

where $A = 3.7 \times 10^5$ MPa, $B = 3.23 \times 10^3$ MPa, $R_1 = 4.15$, $R_2 = 0.95$ and $\omega = 0.3$. $V = \frac{\rho_0}{\rho}$ is the relative volume. The initial density and the specific internal energy is $\rho_0 = 1{,}630\,\text{kg}/m^3$ and $e_0 = 4.3$ MJ/kg, respectively.

The circular plate is made of RHA steel which is governed by the Johnson–Cook constitutive model (Neubergera *et al.*, 2007) in equation (33):

$$\sigma_y = (A + B\varepsilon^{pn})(1 + C\ln\dot{\varepsilon}) \tag{33}$$

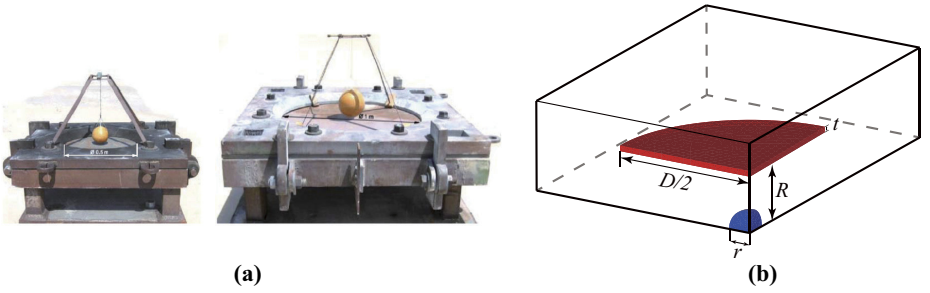

(a) (b)

Figure 9. The experiment devices and the computational model of the blast-plate interaction problem

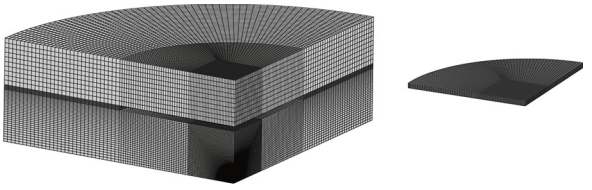

(a) (b)

Figure 10. The fluid and solid grid of the blast-plate interaction problem

where $A = 950\ MPa$, $B = 560\ MPa$, $n = 0.26$ and $C = 0.014$. The Young's modulus and Poisson's ratio of the RHA steel are 210 GPa and 0.28, respectively.

The Johnson–Cook model is incorporated with the Mie–Gruneisen equation of state (Meyers, 1994), namely:

$$p = p_H\left(1 - \frac{\gamma\mu}{2}\right) + \gamma\rho e \tag{34}$$

where $\mu = \frac{\rho}{\rho_0} - 1$ and $\gamma = 1.67$. p_H is calculated from:

$$p_H = \begin{cases} \rho_0 C_0^2\left[\mu + (2S-1)\mu^2 + (S-1)(3S-1)\mu^3\right] & \mu > 0 \\ \rho_0 C_0^2 \mu & \mu < 0 \end{cases}$$

where $\rho_0 = 7{,}850\ \mathrm{kg}/m^3$, $C_0 = 4{,}610$ m/s and $S = 1.49$.

The pressure contour of the fluid in the first 0.1 ms is shown in Figure 11. In this period, the blast wave arrives at the plate and they begin to interact with each other. The explosive wave impacts at the plate around $t = 0.016$ ms and it then propagates alone the radial direction of the plate. Meanwhile, the plate begins to deform gradually.

Figure 12 is the deformation and the equivalent stress of the plate form $t = 0.2$ ms to $t = 0.5$ ms. It shows that the deformation and the magnitude of the equivalent stress increase gradually during the interaction.

Finally, Figure 13 is the curve of the maximal displacement of the plate. The peak displacement is about 24 mm around $t = 0.46$ ms. On the other hand, the experiment result of

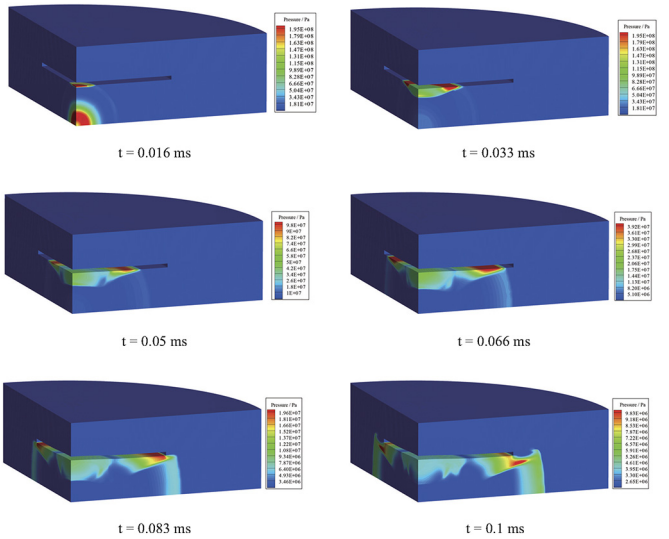

Figure 11.
The interaction between the blast wave and the plate

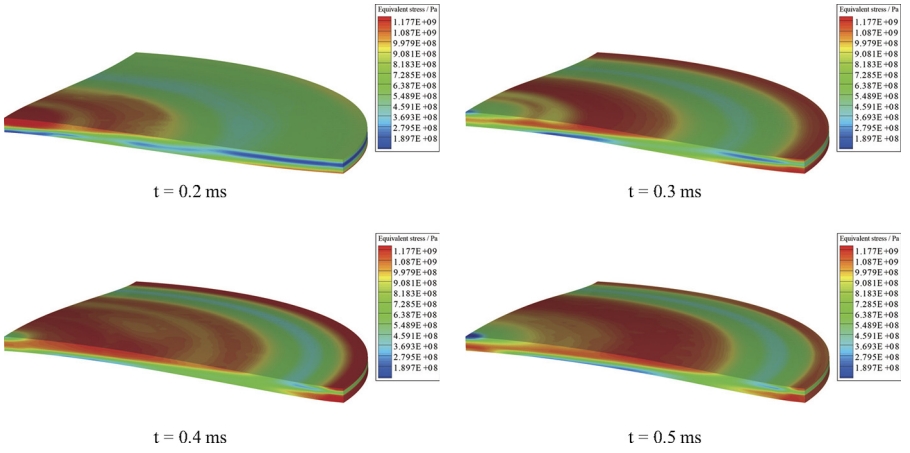

Figure 12.
The deformation and equivalent stress of the plate

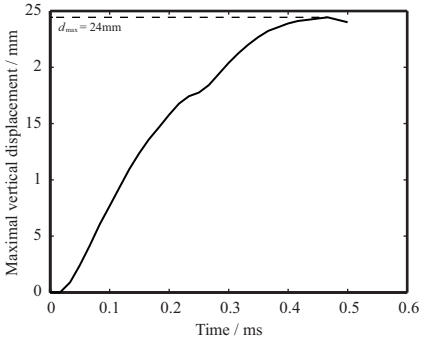

Figure 13.
The curve of the maximal displacement of the plate

the maximal displacement is 26 mm. Our numerical result is close to the experimental data which demonstrates the validity of the MMALE-FE method.

6. Conclusions

The simulation of the fluid solid interaction problem with multi-material flow is an important issue in engineering practice. However, it is also a great challenge in computational mechanics because of difficulties in calculating the interaction and capturing the material interface. In this paper, we present the coupled MMALE-FE method that integrate the multi-material ALE and the FE method to simulate these problems. The coincidence assumption is used on the fluid–solid interfacial nodes and it leads to the accurate calculation of the interacted force. The consistence of the time integration scheme and the rezoning phase are also discussed to guarantee the coincidence requirement in the whole simulation. The CONT test and the blast-plate interaction are simulated by the coupled MMALE-FE method. The numerical results fit well with the benchmark and the experimental data which verify the validity of this method.

References

Ahn, H.T. and Shashkov, M. (2007), "Multi-material interface reconstruction on generalized polyhedral meshes", *Journal of Computational Physics*, Vol. 226 No. 2, pp. 2096-2132.

Barlow, A., Hill, R. and Shashkov, M. (2014), "Constrained optimization framework for interface-aware Sub-scale dynamics closure model for multimaterial cells in Lagrangian and arbitrary Lagrangian-Eulerian hydrodynamics", *Journal of Computational Physics*, Vol. 276, pp. 92-135.

Belytschko, T., Lin, J. and Tasy, C.S. (1983), "Explicit algorithm for nonlinear dynamics of shells", *Computer Methods in Applied Mechanics and Engineering*, Vol. 42 No. 2, pp. 225-251.

Belytschko, T., Wong, B.L. and Chiang, H.Y. (1991), "Advances in on-point quadrature shell elements", *Computer Methods in Applied Mechanics and Engineering*, Vol. 96, pp. 93-107.

Benson, D.J. (1992), "Computational methods in Lagrangian and Eulerian hydrocodes", *Computer Methods in Applied Mechanics and Engineering*, Vol. 99 No. 2-3, pp. 235-394.

Benson, D.J. (2002), "Volume of fluid interface reconstruction methods for multi-material problems", *Applied Mechanics Reviews*, Vol. 55 No. 2, pp. 151-165.

Benuzzi, A. (1987), "Comparison of different LMFBR primary containment codes applied to a benchmark problem", *Nuclear Engineering and Design*, Vol. 100 No. 2, pp. 239-249.

Berndt, M., Breil, J., Galera, S., Kucharik, M., Maire, P.H. and Shashkov, M. (2010), "Two-step hybrid conservative remapping (conservative interpolation) for multimaterial arbitrary Lagrangian-Eulerian method", *Journal of Computational Physics*, Vol. 230 No. 17, pp. 6664-6687.

Blom, F.J. (2000), "Considerations on the spring analogy", *International Journal for Numerical Methods in Fluids*, Vol. 32 No. 6, pp. 647-688.

Caramana, E.J., Burton, D.E., Shashkov, M. and Whalen, P.P. (1998), "The construction of compatible hydrodynamics algorithms utilizing conservation of total energy", *Journal of Computational Physics*, Vol. 146 No. 1, pp. 227-262.

Caramana, E.J. and Shashkov, M. (1998), "Elimination of artificial grid distortion and hourglass-type motions by means of Lagrangian subzonal masses and pressures", *Journal of Computational Physics*, Vol. 142 No. 2, pp. 521-561.

Caramana, E.J. and Loubere, R. (2006), "Curl-q: a vorticity damping artificial viscosity for essentially irrotational Lagrangian hydrodynamics calculations", *Journal of Computational Physics*, Vol. 215 No. 2, pp. 385-391.

Caramana, E.J., Rousculp, C.L. and Burton, D.E. (2000), "A compatible, energy and symmetry preserving Lagrangian hydrodynamics algorithm in three-dimensional Cartesian geometry", *Journal of Computational Physics*, Vol. 157 No. 1, pp. 89-119.

Caramana, E.J., Shashkov, M. and Whalen, P.P. (1998), "Formulations of artificial viscosity for multi-dimensional shock wave computations", *Journal of Computational Physics*, Vol. 144 No. 1, pp. 70-97.

Chen, X. and Zhang, X. (2016), "An improved 3D MoF method based on analytical partial derivatives", *Journal of Computational Physics*, Vol. 326, pp. 156-170.

Chen, X. and Zhang, X. (2017), "An improved 2d MoF method by using high order derivatives", *Journal of Computational Physics*, Vol. 349, pp. 176-190.

Chen, Z.P., Qiu, X.M., Zhang, X. and Lian, Y.P. (2015), "Improved coupling of finite element method with material point method based on a particle-to-surface contact algorithm", *Computer Methods in Applied Mechanics and Engineering*, Vol. 293 No. 15, pp. 1-19.

Chen, X., Zhang, X. and Jia, Z. (2017), "A robust and efficient polyhedron subdivision and intersection algorithm for three-dimensional MMALE remapping", *Journal of Computational Physics*, Vol. 338, pp. 1-17.

Donea, J., Giuliani, S. and Halleux, J.P. (1982), "An arbitrary Langrangian–Eulerian finite element method for transient dynamic fluid-structure interaction", *Computer Methods in Applied Mechanics and Engineering*, Vol. 33 No. 1-3, pp. 689-723.

Fedkiw, R.P., Aslam, T., Merriman, B. and Osher, S. (1999), "A non-oscillatory Eulerian approach to interfaces in multimaterial flows (the ghost fluid method)", *Journal of Computational Physics*, Vol. 152 No. 2, pp. 457-492.

Fedkiw, R.P., Aslam, T. and Xu, S.J. (1999), "The ghost fluid method for deflagration and detonation discountinuities", *Journal of Computational Physics*, Vol. 154 No. 2, pp. 393-427.

Felippa, C.A., Park, K.C. and Farhat, C. (2001), "Partitioned analysis of coupled mechanical systems", *Computer Methods in Applied Mechanics and Engineering*, Vol. 190 No. 24-25, pp. 3247-3270.

Galera, S., Breil, J. and Maire, P.H. (2011), "A 2D unstructured multi-material cell-centered arbitrary Lagrangian-Eulerian (CCALE) scheme using MOF interface reconstruction", *Computers and Fluids*, Vol. 46, pp. 237-244.

Galera, S., Maire, P.H. and Breil, J. (2010), "A two-dimensional unstructured cell-centered multi-material ALE scheme using VOF interface reconstruction", *Journal of Computational Physics*, Vol. 229 No. 16, pp. 5755-5787.

Garimella, R., Kucharik, M. and Shashkov, M. (2007), "An efficient linearity and bound preserving conservative interpolation (remapping) on polyhedral meshes", *Computers and Fluids*, Vol. 36, pp. 224-237.

Grandy, J. (1999), "Conservative remapping and region overlays by intersecting arbitrary polyhedra", *Journal of Computational Physics*, Vol. 148 No. 2, pp. 433-466.

Hirt, C.W., Amsden, A.A. and Cook, J.L. (1997), "An arbitrary Lagrangian-Eulerian computing method for all flow speeds", *Journal of Computational Physics*, Vol. 135 No. 2, pp. 203-216.

Hu, H.H., Patankar, N.A. and Zhu, M.Y. (2001), "Direct numerical simulations of fluid–solid systems using the arbitrary Lagrangian–Eulerian technique", *Journal of Computational Physics*, Vol. 169 No. 2, pp. 427-462.

Huerta, A. and Liu, W.K. (1988), "Viscous flow with large free surface motion", *Computer Methods in Applied Mechanics and Engineering*, Vol. 69 No. 3, pp. 277-324.

Jia, Z.P., Liu, J. and Zhang, S.D. (2013), "An effective integration of methods for second-order three-dimensional multi-material ALE method on unstruced hexahedral meshes using MOF interface reconstruction", *Journal of Computational Physics*, Vol. 236, pp. 513-562.

Kjellgren, P. and Hyvarinen, J. (1998), "An arbitrary Lagrangian-Eulerian finite element method", *Computational Mechanics*, Vol. 21 No. 1, pp. 81-90.

Knupp, P., Margolin, L.G. and Shashkov, M. (2002), "Reference Jacobian optimization-based rezone strategies for arbitrary Lagrangian Eulerian methods", *Journal of Computational Physics*, Vol. 176 No. 1, pp. 93-128.

Kolev, T. and Rieben, R.N. (2009), "A tensor artificial viscosity using a finite element approach", *Journal of Computational Physics*, Vol. 228 No. 22, pp. 8336-8366.

Kucharik, M. and Shashkov, M. (2012), "One-step hybrid remapping algorithm for multi-material arbitrary Lagrangian-Eulerian method", *Journal of Computational Physics*, Vol. 231 No. 7, pp. 2851-2864.

Kucharik, M. and Shashkov, M. (2014), "Conservative multi-material remap for staggered multi-material arbitrary-Lagrangian-Eulerian methods", *Journal of Computational Physics*, Vol. 258, pp. 268-304.

Kucharik, M., Garimella, R.V., Schofield, S.P. and Shashkov, M. (2010), "A comparative study of interface reconstruction methods for multi-material ALE simulations", *Journal of Computational Physics*, Vol. 229 No. 7, pp. 2432-2452.

Kucharik, M., Shashkov, M. and Wendroff, B. (2003), "An efficient linearity-and-bound-preserving remapping method", *Journal of Computational Physics*, Vol. 188 No. 2, pp. 462-471.

Lian, Y.P., Liu, Y. and Zhang, X. (2011), "Coupling of finite element method with material point method by local multi-mesh contact method", *Computer Methods in Applied Mechanics and Engineering*, Vol. 200 Nos 47/48, pp. 3482-3494.

Lian, Y.P., Liu, Y. and Zhang, X. (2012), "Coupling between finite element and material point method for problems with extreme deformation", *Theoretical and Applied Mechanics Letters*, Vol. 2, pp. 021003.

Lian, Y.P., Liu, Y. and Zhang, X. (2014), "Coupling of membrane element with material point method for fluid membrane interaction problems", *International Journal of Mechanics and Materials in Design*, Vol. 10 No. 2, pp. 199-211.

Liu, M.B., Liu, G. and Lam, K.Y. (2003), "Meshfree particle simulation of the detonation process for high explosive in shaped unlined cavity configurations", *Shock Waves*, Vol. 12 No. 6, pp. 509-520.

Liu, W.K. and Ma, D.C. (1982), "Computer implementation aspects for fluid-structure interaction problems", *Computer Methods in Applied Mechanics and Engineering*, Vol. 31 No. 2, pp. 129-148.

Liu, W.K., Liu, Y.L., Farrell, D., Zhang, L.T., Wang, S., Fukui, Y., Patankar, N., Zhang, Y.J., Bajaj, C., Lee, J., Hong, J. and Hus, H.Y. (2006), "Immersed finite element method and its applications to biological systems", *Computer Methods in Applied Mechanics and Engineering*, Vol. 195 Nos 13/16, pp. 1722-1749.

Loubere, R., Maire, P.H. and Vachal, P. (2013), "3D staggered Lagrangian hydrodynamics scheme with cell-centered Riemann solver-based artificial viscosity", *International Journal for Numerical Methods in Fluids*, Vol. 72, pp. 22-42.

Luo, H., Baum, J.D. and Lohner, R. (2004), "On the computation of multi-material flows using ALE formulation", *Journal of Computational Physics*, Vol. 194 No. 1, pp. 304-328.

Meyers, M.A. (1994), *Dynamic Behavior of Materials*, John Wiley and Son.

Neubergera, A., Peles, S. and Rittel, D. (2007), "Scaling the response of circular plates subjected to large and close-range spherical explosions. Part i air-blast loading", *International Journal of Impact Engineering*, Vol. 32, pp. 859-873.

Peery, J.S. and Carroll, D.E. (2000), "Multi-material ALE methods in unstructured grids", *Computer Methods in Applied Mechanics and Engineering*, Vol. 187 Nos 3/4, pp. 591-619.

Piperno, S. and Farhat, C. (2001), "Partitioned procedures for the transient solution of coupled aeroelastic problems - part ii: energy transfer analysis and three-dimensional applications", *Computer Methods in Applied Mechanics and Engineering*, Vol. 190 Nos 24/25, pp. 3147-3170.

Piperno, S., Farhat, C. and Larrouturou, B. (1995), "Partitioned procedures for the transient solution of coupled aeroelastic problems – part i: Model problem, theory and two-dimensional applications", *Computer Methods in Applied Mechanics and Engineering*, Vol. 124 Nos 1/2, pp. 79-112.

Robbea, M.F., Lepareux, M., Treille, E. and Cariou, Y. (2003), "Numerical simulation of a hypothetical core disruptive accident in a small-scale model of a nuclear reactor", *Nuclear Engineering and Design*, Vol. 233, pp. 159-196.

Shashkov, M. (2008), "Closure models for multimaterial cells in arbitrary Lagrangian-Eulerian hydrocodes", *International Journal for Numerical Methods in Fluids*, Vol. 56, pp. 1479-1504.

Vitali, E. and Benson, D.J. (2006), "An extended finite element formulation for contact in multi-material arbitrary Lagrangian-Eulerian calculation", *International Journal for Numerical Methods in Engineering*, Vol. 67 No. 10, pp. 1420-1444.

Wang, X.S. and Zhang, L.T. (2013), "Modified immersed finite element method for fully-coupled fluid-structure interactions", *Computer Methods in Applied Mechanics and Engineering*, Vol. 267, pp. 150-169.

William, J.R. and Douglas, B.K. (1998), "Reconstructing volume tracking", *Journal of Computational Physics*, Vol. 121, pp. 112-152.

Yanilkin, Y.V., Goncharov, E.A., Kolobyanin, V.Y., Sadchikov, V.V., Kamm, J.R., Shashkov, M. and Rider, W.J. (2013), "Multi-material pressure relaxation methods for Lagrangian hydrodynamics", *Computers and Fluids*, Vol. 83, pp. 137-143.

Yoseph, P.Z., Mereu, S., Chippada, S. and Kalro, V.J. (2001), "Automatic monitoring of element shape quality in 2-D and 3-D computational mesh dynamics", *Computational Mechanics*, Vol. 27, pp. 378-395.

Zhang, L.T., Gerstenberger, A., Wang, X.D. and Liu, W.K. (2004), "Immersed finite element method", *Computer Methods in Applied Mechanics and Engineering*, Vol. 193 Nos 21/22, pp. 2051-2067.

Zhang, L.T., Wagner, G.J. and Liu, W.K. (2003), "Modelling and simulation of fluid structure interaction by meshfree and FEM", *Communications in Numerical Methods in Engineering*, Vol. 8, pp. 615-621.

Zhang, F., Zhang, X., Sze, K.Y., Lian, Y.P. and Liu, Y. (2017), "Incompressible material point method for free surface flow", *Journal of Computational Physics*, Vol. 330, pp. 92-110.

Corresponding author
Dr Xiong Zhang can be contacted at: xzhang@tsinghua.edu.cn